Oscillatory Notch-pathway activity in a delay model of neuronal differentiation

Hiroshi Momiji*
Department of Biomedical Science, University of Sheffield, Western Bank, Sheffield S10 2TN, United Kingdom

Nicholas A. M. Monk†
School of Mathematical Sciences, University of Nottingham, University Park, Nottingham NG7 2RD, United Kingdom

(Received 9 February 2009; published 24 August 2009)

Lateral inhibition resulting from a double-negative feedback loop underlies the assignment of different fates to cells in many developmental processes. Previous studies have shown that the presence of time delays in models of lateral inhibition can result in significant oscillatory transients before patterned steady states are reached. We study the impact of local feedback loops in a model of lateral inhibition based on the Notch signaling pathway, elucidating the roles of intracellular and intercellular delays in controlling the overall system behavior. The model exhibits both in-phase and out-of-phase oscillatory modes and oscillation death. Interactions between oscillatory modes can generate complex behaviors such as intermittent oscillations. Our results provide a framework for exploring the recent observation of transient Notch-pathway oscillations during fate assignment in vertebrate neurogenesis.

DOI: 10.1103/PhysRevE.80.021930 PACS number(s): 87.18.Vf, 02.30.Ks, 87.16.Xa, 87.16.Yc

I. INTRODUCTION

As in many electronic circuits, classes of oscillators and switches are fundamental elements in many gene regulatory networks [1,2]. In particular, a double-negative feedback loop comprising two mutually repressive components is known to be capable of functioning as a toggle switch, allowing a system to adopt one of the two possible steady states (corresponding to cell fates) [3,4]. In the context of developmental biology, such bistable switch networks can operate between cells and are believed to drive cell differentiation in a wide range of contexts. However, in naturally evolved (rather than engineered) gene regulatory networks, double-negative feedback loops rarely exist in a "pure" form, and interactions between loop components and other network components often result in sets of interconnected feedback loops. Furthermore, if loop interactions involve the regulation of gene expression, then interactions are delayed rather than instantaneous. The present study investigates the dynamic behavior of a double-negative feedback loop when the nodes of the loop are involved in additional feedback loops and when the regulatory steps constituting the resulting network involve significant time delays.

A particularly well-documented example of a biological double-negative feedback loop is centered on transmembrane receptors of the Notch family. Notch signaling, resulting from direct interaction with transmembrane ligands of the Delta, Serrate, and Lag-2 (DSL) family on neighboring cells mediates an evolutionarily conserved lateral inhibition mechanism that operates to specify differential cell fates during many developmental processes [5–8]. Although gene nomenclature varies between different organisms, a core circuitry—the neurogenic network—underlying lateral inhibition can be identified and is illustrated schematically in Fig. 1 [9,10]. In brief, signaling between neighboring cells is mediated by direct (juxtacrine) interactions between Notch receptors and DSL ligands. A double-negative feedback loop is formed by the repression of DSL ligand activity by Notch signaling in the same cell (cell autonomous repression) [Fig. 1(a)]. Mathematical models of such a spatially distributed double-negative feedback loop are capable of generating robust spatial patterns of Notch signaling in populations of cells [9].

In many developmental settings, the level of Notch signaling regulates the fate adopted by a cell by acting as an input to a cell autonomous bistable switch formed by one or more proneural genes (such as *achaete* and *scute* in *Drosophila* and *neurogenin* and *atonal* in vertebrates) [11]. The

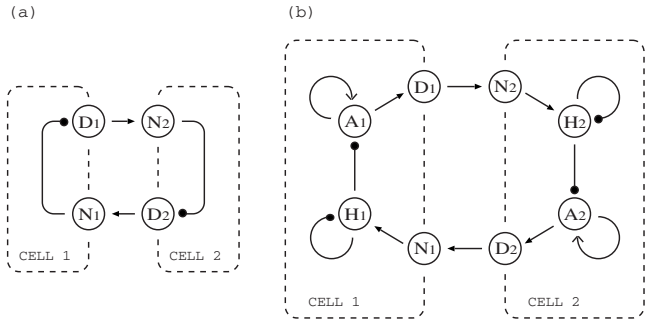

FIG. 1. The neurogenic network models in a two-cell representation. The letters on the nodes correspond to the key classes of protein involved in the network. D: DSL ligand, N: Notch receptor, H: Hes-Her proteins, A: proneural proteins (e.g., Achaete, Scute, and Neurogenin). Edges represent two types of directional interactions: activation (→) and repression (⊣). (a) The pure double-negative feedback loop involving only DSL ligand and Notch receptor [9,15]. (b) A more detailed model that incorporates Hes-Her negative feedback and proneural positive feedback [10].

*Present address: Warwick Systems Biology Centre, University of Warwick, Coventry CV4 7AL, UK, and Warwick HRI, University of Warwick, Wellesbourne, Warwick CV35 9EF, UK. h.momiji@warwick.ac.uk
†nick.monk@nottingham.ac.uk

basic principle underlying this switch is the ability of the protein products of the proneural genes to positively regulate transcription of proneural genes, resulting in a direct positive feedback loop. In many systems, including the developing nervous system, Notch signaling regulates the proneural switch via regulation of the expression of proteins of the Hes-Her family. These proteins act as transcriptional repressors and can repress their own expression and interfere with proneural self-activation [12]. Furthermore, proneural proteins can also positively regulate the expression of DSL proteins, forming a complete circuit of interactions as shown in Fig. 1(b). Considered as an intercellular signaling network—which we shall refer to as the neurogenic network—this circuit comprises a spatially distributed double-negative feedback loop with additional local positive and negative feedback loops.

A detailed mathematical model of the neurogenic network, incorporating Hes-Her negative feedback and proneural positive feedback, has been studied by Meir *et al.* [10], who showed by computer simulation that the network is capable of generating spatial patterns of Notch signaling in populations of cells. The models of Collier *et al.* [9] and Meir *et al.* [10] incorporate the implicit assumption that all interactions are nondelayed. However, in reality the basic production mechanisms that regulate gene expression (gene transcription and translation) are associated with time delays [13,14]. Incorporation of explicit time delays in the pure double-negative feedback loop shown in Fig. 1(a) results in a competition between dynamic modes, with a stable spatial patterning typically preceded by significant oscillatory transients [15]. In a biological context, such transients would play an important role in delaying the onset of cell differentiation in a developing tissue. Delays can also generate oscillatory dynamics in models of Hes-Her negative feedback loops [16–19], and such oscillations have been observed experimentally [12,20,21].

As predicted by mathematical models [15,17], oscillatory expression of DSL ligands, Hes-Her proteins, and proneural proteins has recently been observed in neural precursors in the developing mouse brain [22]. Furthermore, these oscillations have been predicted to play a central biological role in delaying the onset of neural differentiation [22]. In principle, these oscillations could be driven by the cell autonomous Hes-Her negative feedback loop, with Notch signaling providing coupling between cells [17], or by the double-negative feedback loop centered on the DSL-Notch interaction [15]. In the following, we investigate the interplay between local and intercellular feedback loops in models of the neurogenic network, using a combination of linear stability analysis and numerical simulations, emphasizing the dynamical effects of the multiple time delays in the network. We study principally the case of two coupled cells, since this captures the essential features of oscillator synchronization and cell state differentiation. We also show how our results extend to larger populations of coupled cells.

II. FULL Hes-Her–PRONEURAL MODEL AND ITS DISSECTION

In Fig. 1(b), positive regulation of Hes-Her (H) by proneural protein (A) in the adjacent cell, mediated by DSL-

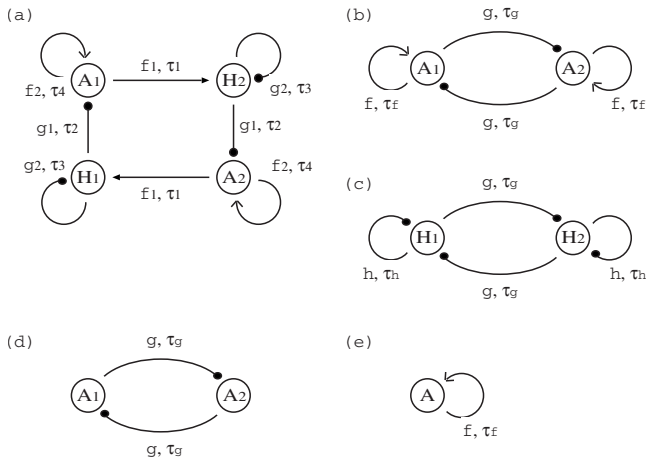

FIG. 2. The neurogenic network models examined in the present study. τ: time delays, f: a general increasing function; g,h: general decreasing functions. With an appropriate choice of time delay (τ_1), the model in (a) provides a simplified representation of the full model shown in Fig. 1(b). The models in (a)–(d) have the potential to exhibit both oscillations and differentiation, while the model in (e) exhibits only differentiation.

Notch signaling can be considered simply as a cascade of three low-pass filters. This simplification allows the model in Fig. 1(b) to be reduced to the model in Fig. 2(a), where τ denotes time delay, and f and g represent generic increasing and decreasing functions, respectively. In this model, referred to hereafter as the full Hes-Her–proneural model, Hes-Her proteins repress proneural proteins in the same cell (1 or 2), while proneural proteins activate Hes-Her proteins in the adjacent cell. This main loop is supplemented by the two local loops: Hes-Her autorepression and proneural autoactivation. Each interaction is not instantaneous but involves a time delay, typically on the order of minutes to tens of minutes [15–18]. The delays in the cell-autonomous regulatory steps ($\tau_2-\tau_4$) originate predominantly from processes associated with gene transcription, whereby the DNA sequence of a gene is transcribed into a corresponding mRNA molecule, while the delay in the non-cell-autonomous interaction (τ_1) represents in addition processes involved in DSL-Notch signaling, such as protein processing [23].

The models in Figs. 2(b)–2(e) are obtained by a sequential reduction in the full neurogenic network. When Hes-Her feedback is negligible, the full Hes-Her–proneural model in Fig. 2(a) becomes the model in Fig. 2(b); while when proneural feedback is negligible, the model in Fig. 2(a) becomes the model in Fig. 2(c). When both local loops are negligible, models (b) and (c) can be reduced to the model in Fig. 2(d). Finally, because two sequential repressions function as a net activation, the model in Fig. 2(d) can be further reduced to the model in Fig. 2(e). Such simple network elements appear repeatedly in gene regulatory networks (and possibly in other biological and nonbiological networks) and are examples of what are often called "motifs" [24]. The models in Figs. 2(b)–2(e) are called hereafter as (b) the autoactivation two-proneural model, (c) the autorepression two-Hes-Her model, (d) the nonautonomous proneural model, and (e) the autoactivation single-proneural model.

III. MATHEMATICAL REPRESENTATION OF THE FULL Hes-Her–PRONEURAL MODEL

We represent Hes-Her and proneural proteins by a single variable in each cell. To investigate the behavior of a network quantitatively, it is convenient to scale each variable such that it lies in the range [0,1]. The full Hes-Her–proneural model [Fig. 2(a)] can then be represented by the following differential equations with discrete delays:

$$T_H\dot{H}_1 = -H_1 + P_H[A_2(t-\tau_1), H_1(t-\tau_3)], \tag{1}$$

$$T_A\dot{A}_1 = -A_1 + P_A[H_1(t-\tau_2), A_1(t-\tau_4)], \tag{2}$$

$$T_H\dot{H}_2 = -H_2 + P_H[A_1(t-\tau_1), H_2(t-\tau_3)], \tag{3}$$

$$T_A\dot{A}_2 = -A_2 + P_A[H_2(t-\tau_2), A_2(t-\tau_4)], \tag{4}$$

where T_H and T_A denote the degradation constants (the inverses of the linear degradation rates) of H and A, respectively [10]. P_H and P_A are functions representing the rates of production of H and A, respectively. The activating and the repressive actions of the proneural and the Hes-Her proteins are captured by the following constraints:

$$\frac{\partial P_H}{\partial A} > 0, \quad \frac{\partial P_H}{\partial H} < 0, \tag{5}$$

$$\frac{\partial P_A}{\partial A} > 0, \quad \frac{\partial P_A}{\partial H} < 0. \tag{6}$$

For our analysis of this and the reduced models, we need assume no more about the production functions than conditions (5) and (6). For numerical simulations, specific functional forms must be assumed, and we take these functions to be products of increasing (f) and decreasing (g or h) Hill functions. Specifically, we assume that $P_I(A,H)=f_I(A)g_I(H)$ for $I=A$ or H, where

$$f_I(x,K,\nu) = \frac{x^\nu}{K^\nu + x^\nu}, \tag{7}$$

$$g_I(x,K,\nu) = \frac{K^\nu}{K^\nu + x^\nu}, \tag{8}$$

and K and ν represent the scaled threshold and the Hill coefficient, respectively. However, the qualitative behavior of the model solutions is preserved for other choices of production functions that satisfy conditions (5) and (6).

Numerical simulations of this model reveal a range of qualitatively different types of behavior, in which oscillations can be absent, transient, or sustained, and their phases can be locked or not (for examples, see Fig. 3). To investigate the origin of these behaviors, we reduce the full Hes-Her–proneural model to a variety of simpler ones (see Fig. 2). The examination of these simpler networks (motifs) helps one to elucidate the origins of the dynamics of the full Hes-Her–proneural model.

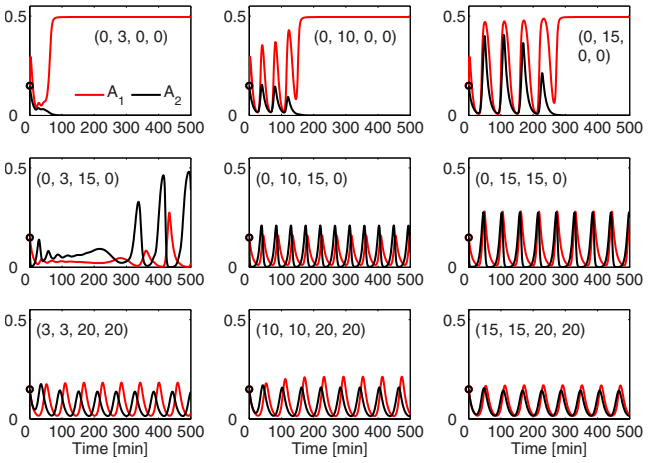

FIG. 3. (Color online) Examples of typical dynamics found in numerical simulations of the full Hes-Her–proneural model shown in Fig. 2(a) and defined by Eqs. (1)–(8), displaying both differentiation and oscillations. Oscillations can be transient or sustained and can be in phase between two cells, or not. Values of the kinetic parameters are set the same on each row and listed in Table I. Delays are given in each panel as $(\tau_1,\tau_2,\tau_3,\tau_4)$

IV. ANALYSIS AND SIMULATION OF REDUCED MODELS

In this study, we are concerned primarily with the routes that cells take to differentiation. For all model variants, a uniform steady state exists ($H_1^*=H_2^*$, $A_1^*=A_2^*$). Biologically, this corresponds to a nondifferentiated state (i.e., the neurogenic network is in the same state in both cells). We therefore study the stability of this steady state to small perturbations, and we seek to determine the resulting dynamical behavior of the system in cases where it is unstable.

For each model variant [Figs. 2(b)–2(e)], we first perform linear stability analysis of the uniform steady state, which yields an eigenvalue equation. We then determine parameter values that result in the existence of neutral (pure imaginary) eigenvalues, which are the product of the imaginary unit number and the neutral angular frequency, and are associated with changes in stability. To confirm the nature of bifurcations associated with these eigenvalues, the linear analysis is followed by numerical simulations. The eigenvalue equation for each model variant is derived directly from its own model equations, rather than by reduction in the full Hes-Her–proneural model. The conditions under which the full Hes-Her–proneural model can be reduced to the autoactivation two-proneural model and to the autorepression two-Hes-Her model are discussed in Sect. VI.

To allow systematic comparison between model variants, we use a standard set of parameter values—which are listed in Table I—in both analysis and simulations. These parameter values fall into a biologically reasonable range [10,17] and result in representative model dynamics. Deviations from this standard set are noted explicitly. The time is measured in minutes, yielding values for the degradation constants that are in line with measured values for proneural and neurogenic factors [20,25]. However, the behavior of each model variant is also examined with other parameter values.

TABLE I. Parameter values.

		f_H		g_H			g_A		f_A	
	T_H	K	ν	K	ν	T_A	K	ν	K	ν
Standard	10	0.01	2	0.01	2	10	0.01	2	0.01	2
Figure 3										
Top	1	0.1	2	0.1	0	10	0.01	2	0.01	2
Middle	10	0.1	2	0.01	2	1	0.01	2	0	0
Bottom	10	0.01	2	0.01	2	10	0.01	2	0.01	2

In the following analyses, γ denotes the *magnitude* of the slope of the regulatory function $[f_{j=1,2}(x)$ or $g_{j=1,2}(x)]$ at the uniform steady-state solution $(H^*_{i=1,2}$ or $A^*_{i=1,2})$. In the cases of the Hill functions

$$\gamma^{g_{j=1,2}}_{i=1,2} = - \left.\frac{dg_{j=1,2}}{dx_i}\right|_{x_i^*} = \frac{\nu K^\nu x_i^{*\nu-1}}{(K^\nu + x_i^{*\nu})^2} > 0, \tag{9}$$

$$\gamma^{f_{j=1,2}}_{i=1,2} = + \left.\frac{df_{j=1,2}}{dx_i}\right|_{x_i^*} = \frac{\nu K^\nu x_i^{*\nu-1}}{(K^\nu + x_i^{*\nu})^2} > 0, \tag{10}$$

where, in general, K and ν are different in $f_{j=1,2}(x)$ and in $g_{j=1,2}(x)$, and therefore $\gamma^{g_{j=1,2}}_{i=1,2} \neq \gamma^{f_{j=1,2}}_{i=1,2}$. In the following sections, it can be seen that what determines the stability properties of the homogeneous steady state is not the precise functional forms of f and g, but the value of γ.

A. Nonautonomous two-proneural model

The nonautonomous two-proneural model [Fig. 2(d)] is represented by the following differential equations:

$$T\dot{A}_1 = -A_1 + g(A_2(t-\tau)), \tag{11}$$

$$T\dot{A}_2 = -A_2 + g(A_1(t-\tau)). \tag{12}$$

To study the stability of the uniform steady-state solution $(A_1^*=A_2^*=A^*)$, we set $A_1(t)=A^*+a_1(t)$ and $A_2(t)=A^*+a_2(t)$ in Eqs. (11) and (12). Following linearization, the resulting coupled equations for a_1 and a_2 can be uncoupled by introducing variables a_1+a_2 and a_1-a_2 [9]. The eigenvalue equations derived from the equations in these variables are

$$1 + T\lambda = \pm \gamma e^{-\lambda\tau}, \tag{13}$$

where the plus and the minus branches are associated with a_1-a_2 and a_1+a_2, respectively.

We consider first uniform perturbations such that $a_1=a_2$. In this case, only the minus branch of Eq. (13) is relevant. Assuming a pure imaginary eigenvalue $\lambda=i\omega_c$, with ω_c real, the neutral angular frequency (ω_c) is derived to be

$$\omega_c = \frac{1}{T}\sqrt{\gamma^2 - 1}. \tag{14}$$

This eigenvalue occurs for parameter values such that $\gamma>1$ and when the delay is equal to the neutral delay τ_c,

$$\tau_c = \frac{1}{\omega_c}[\pi + \tan^{-1}(-T\omega_c)]. \tag{15}$$

For the standard set of parameter values (Table I), the oscillatory period associated with the neutral eigenvalue (the Hopf period)—defined by $T_c=2\pi/\omega_c$—is found to be 38.6501 min, while $\tau_c=13.0548$ min. For $\tau\neq\tau_c$, the minus branch of Eq. (13) has a complex eigenvalue with a real part that has the same sign as $\tau-\tau_c$. This can be seen in the numerical solution of Eq. (13) in Fig. 4.

The linear stability analysis suggests that the uniform steady state becomes unstable to small uniform perturbations via a Hopf bifurcation if $\gamma>1$ and the delay increases above the critical value. Numerical simulations of Eqs. (11) and (12) for $\tau>\tau_c$ are shown in Fig. 5. For uniform initial conditions $[A_1(0)=A_2(0)]$ the system exhibits sustained oscillations [Fig. 5(a)]. This confirms that the neutral solution on the minus branch of Eq. (13) is a Hopf bifurcation point.

The plus branch of Eq. (13), which is associated with a_1-a_2, has the same neutral angular frequency (ω_c) as the mi-

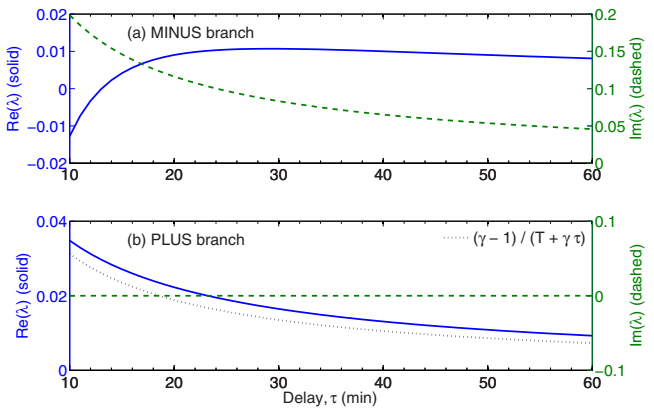

FIG. 4. (Color online) The eigenvalues (λ) of the nonautonomous two-proneural model [Fig. 2(d)] as a function of delay (τ). The eigenvalue equation [Eq. (13)] has two branches. (a) On the minus branch Re(λ) changes its sign from negative to positive as τ surpasses its critical value $(\tau_c=13.0548)$, leading to a Hopf bifurcation, (b) while on the plus branch it is always positive. The minus and the plus branches therefore define, respectively, the oscillatory and the differentiating properties of the system. The dotted line in (b) shows the approximate analytical value for the real part of the eigenvalue derived in Eq. (17).

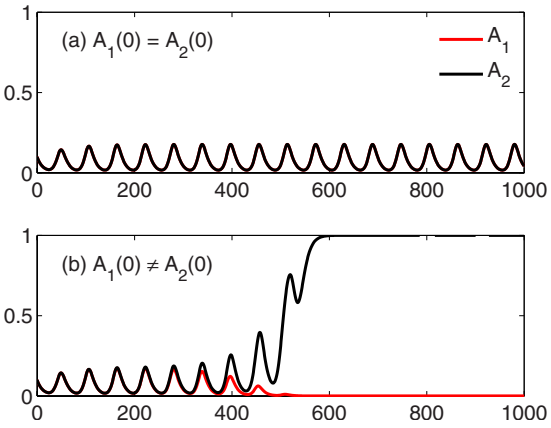

FIG. 5. (Color online) Numerical simulations of the nonautonomous two-proneural model [Fig. 2(d)]. (a) With identical initial values, A_1 and A_2 show sustained in-phase oscillations. (b) With slightly different initial values, A_1 and A_2 show transient in-phase oscillations followed by differentiation (cf. [15]). Standard parameter values are used, as listed in Table I, with $\tau=20$ min.

nus branch, and the neutral eigenvalue occurs for a neutral delay τ_c,

$$\tau_c = \frac{1}{\omega_c}\tan^{-1}(T\omega_c), \tag{16}$$

which takes the value of 6.2702 min for the standard parameter set. More generally, the real part of a complex eigenvalue λ_+ satisfies

$$1 + T\,\mathrm{Re}(\lambda_+) = \gamma e^{-\mathrm{Re}(\lambda_+)\tau}\cos[\mathrm{Im}(\lambda_+)\tau].$$

Since $\mathrm{Re}(\lambda_+)$ is given by the intersection of $y=1+T\,\mathrm{Re}(\lambda_+)$ and $y=\gamma\exp[-\mathrm{Re}(\lambda_+)\tau]\cos[\mathrm{Im}(\lambda_+)\tau]$ on the y-$\mathrm{Re}(\lambda_+)$ plane, a purely real λ_+ (for which $\cos[\mathrm{Im}(\lambda_+)\tau]=1$) has the largest real part and is positive for all values of τ if $\gamma>1$. This positive real eigenvalue is shown in Fig. 4(b). By assuming a purely real eigenvalue (λ_{R+}), and by applying the first-order Taylor expansion to Eq. (13), a simple approximate (lower bound) expression for λ_{R+} is derived to be

$$\lambda_{R+} \simeq \frac{\gamma-1}{T+\gamma\tau}, \tag{17}$$

which is confirmed to provide a good approximation to the growth rate of patterns obtained in numerical simulations in Fig. 4(b). Previously, such an approximation was thought to be possible only in the limit of a large Hill coefficient (ν) [15], while in Fig. 4, $\nu=2$.

The positive real eigenvalue on the plus branch corresponds to differentiation of the two cells (exponential growth of a_1-a_2), while the complex eigenvalue associated with the minus branch corresponds to oscillations (in a_1+a_2). Thus, if $A_1(0)$ and $A_2(0)$ are set slightly different, the behavior of the system comprises a combination of these two fundamental modes. This can be seen in the numerical simulation of Eqs. (11) and (12) in Fig. 5(b), which shows a transient uniform oscillation followed by differentiation. Since the oscillations occur on the minus branch corresponding to a_1+a_2, the oscillatory profiles of A_1 and A_2 are in phase. Similar transient

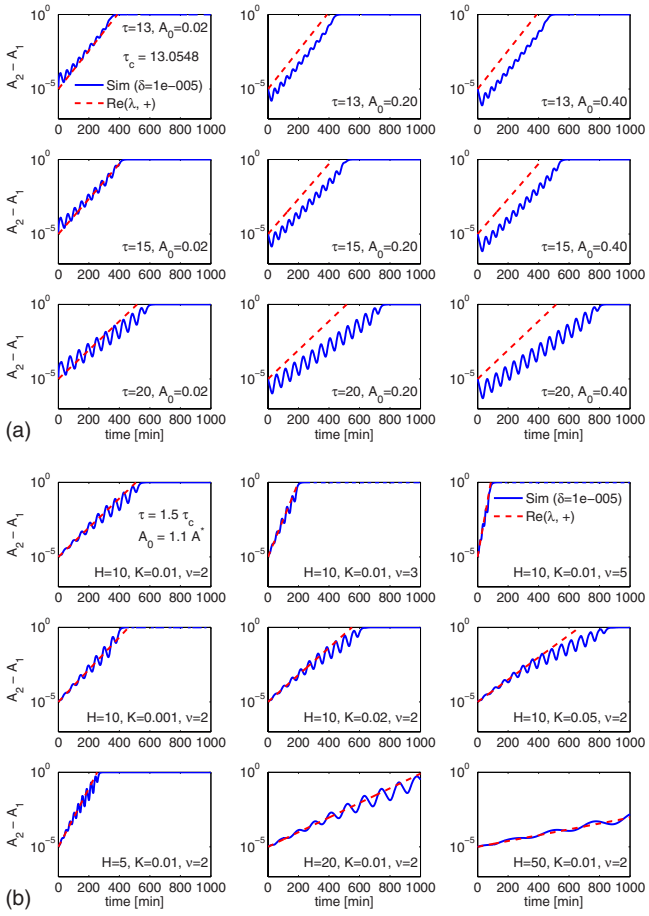

FIG. 6. (Color online) Time taken for differentiation in the nonautonomous two-proneural model [Fig. 2(d)]. Time courses of the difference A_2-A_1, obtained from numerical simulations, plotted on a logarithmic scale (a) for various delays (τ) and initial mean values ($A_0=0.5[A_2(0)+A_1(0)]$) with the standard parameter set and (b) for various parameter sets with $\tau=1.5\tau_c(H,K,\nu)$, where τ_c is the critical delay. The time courses are compared to the growth rate predicted from linear analysis (dashed line), based on the real part of the eigenvalue [Re(λ)].

oscillations leading to differentiation have been observed previously in a delay model of the Delta-Notch signaling system [Fig. 1(a)] [15].

In general, the outcome of linear stability analysis is not applicable to transient system behavior. Therefore, the separation of the two branches makes linear analysis highly valuable in this study, making possible the prediction of whether or not a transient oscillation leading to differentiation occurs. More striking is the fact that not only the initial rate of differentiation, but also the time taken to complete differentiation can be estimated by linear analysis. Figure 6 shows the time courses of the (logarithmic) difference A_2-A_1 obtained from numerical simulations for a range of values of the delay (τ) and initial mean values ($A_0=0.5[A_2(0)+A_1(0)]$). These are compared to the growth rate predicted by the real part of the eigenvalue for a_2-a_1 (i.e., the plus branch), obtained from linear analysis for the corresponding τ (Fig. 4), which provides a good estimate of the time taken to reach the fully differentiated state.

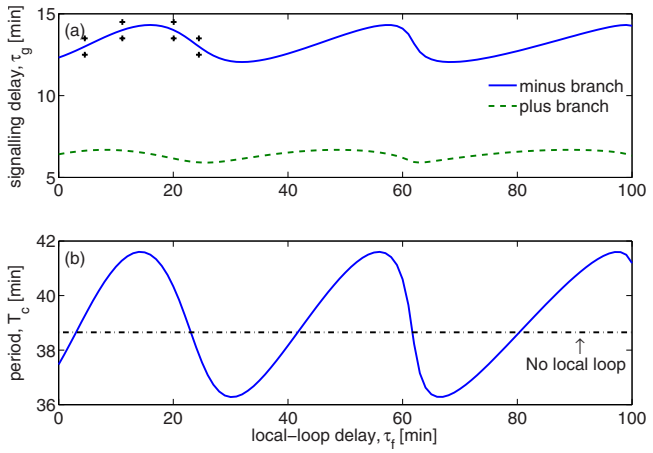

FIG. 7. (Color online) Neutral (a) intercellular signaling delay and (b) oscillatory period associated with the pure imaginary eigenvalues of the autoactivation two-proneural model [Fig. 2(b)], shown as a function of the local-loop delay (τ_f). The eigenvalue equation [Eq. (21)] is solved numerically for its minus and plus branches. The Hopf bifurcation occurs on the minus branch. Also shown in (b) is the corresponding Hopf period for the nonautonomous two-proneural model, which lacks the local (cell-autonomous) proneural feedback loops [Fig. 2(d)]. Numerical simulations performed for parameter values corresponding to the cross signs in (a) confirm that the Hopf bifurcation occurs on the minus branch of Eq. (21), and that the critical intercellular signaling delay (τ_g) is modulated by τ_f.

B. Autoactivation single-proneural model

Because two sequential repressions result in a net activation, the nonautonomous two-proneural model [Fig. 2(d)] may seem to be surrogated by the autoactivation single-proneural model [Fig. 2(e)], represented by the following differential equation:

$$T\dot{A} = -A + f(A(t-\tau_f)). \tag{18}$$

The eigenvalue equation obtained by linearization about a steady state of Eq. (18) is

$$1 + T\lambda = \gamma e^{-\lambda\tau},$$

which is identical to the plus branch of Eq. (13) that represents the differentiating nature of the nonautonomous two-proneural model. It is therefore clear that the oscillation in the two-proneural model is due to the network structure that two-proneural proteins are mutually repressing.

C. Autoactivation two-proneural model

The autoactivation two-proneural model [Fig. 2(b)] is represented by the following differential equations:

$$T\dot{A}_1 = -A_1 + g(A_2(t-\tau_g))f(A_1(t-\tau_f)), \tag{19}$$

$$T\dot{A}_2 = -A_2 + g(A_1(t-\tau_g))f(A_2(t-\tau_f)). \tag{20}$$

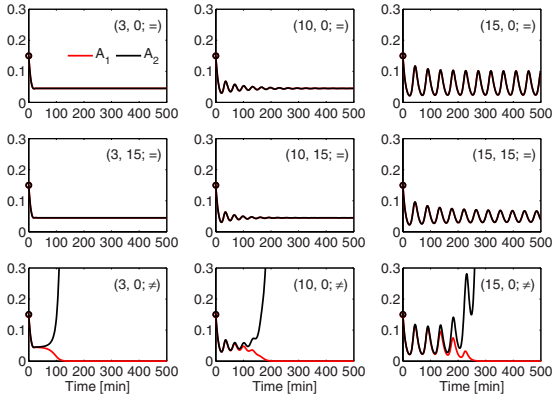

FIG. 8. (Color online) Numerical simulations of the autoactivation two-proneural model [Fig. 2(b)]. In comparison to Fig. 5, the behavior is found to be qualitatively the same as that of the nonautonomous two-proneural model [Fig. 2(d)]. However, the modulatory effect of the cell-autonomous proneural loop, shown in Fig. 7, is seen in comparison between the top and the middle right panels. As the local-loop delay (τ_f) increases from 0 to 15, the amplitude of oscillations decreases, as influenced by the increase in the critical signaling delay [Fig. 7(a), solid curve]. Values of the delays, and whether or not the initial values of A_1 and A_2 are equal, are specified in each panel as (τ_g, τ_f; =or≠).

The eigenvalue equation for the uniform steady-state solution ($A_1^*=A_2^*=A^*$) is derived to be

$$1 + T\lambda = g(A^*)\gamma^f e^{-\lambda\tau_f} \pm f(A^*)\gamma^g e^{-\lambda\tau_g}. \tag{21}$$

The purely imaginary solution $\lambda = i\omega$ satisfies

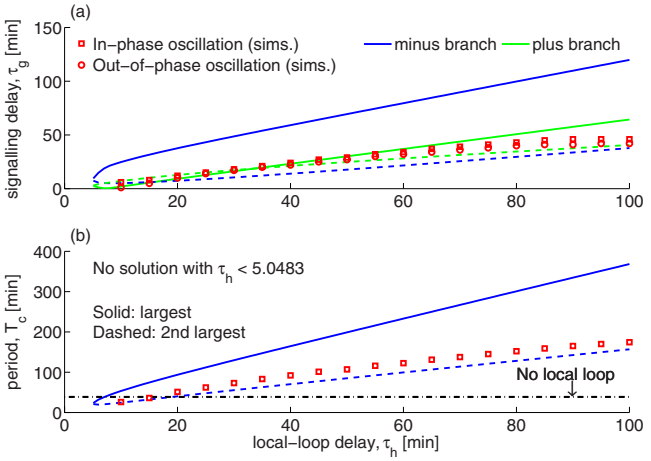

FIG. 9. (Color online) Neutral (a) intercellular signaling delay and (b) oscillatory period associated with the pure imaginary eigenvalues of the autorepression two-Hes-Her model [Fig. 2(c)], shown as a function of the local-loop delay. The eigenvalue equation [Eq. (25)] is solved for its minus and plus branches, for the first and the second largest periods (solid and dashed lines, respectively). This model shows the transition between out-of-phase and in-phase oscillations. At each local-loop delay, a square represents the in-phase oscillation observed in simulation with the lowest signaling delay, while a circle represents the out-of-phase oscillation observed in simulation with the highest signaling delay. The transition happens between them (upper panel), which are overlapping with a square being always above a circle.

$$1 + B^2 - C^2 + T^2\omega^2 + 2B(T\omega \sin \omega\tau_f - \cos \omega\tau_f) = 0, \tag{22}$$

where $B = g(A^*)\gamma^f$ and $C = f(A^*)\gamma^g$.

Figure 7 shows the neutral intercellular signaling delay and the corresponding oscillatory period, associated with the pure imaginary eigenvalues, as a function of local-loop delay (τ_f). The eigenvalue equation [Eq. (21)] is solved for its minus and plus branches. As τ_f is varied, the values of the neutral intercellular signaling delay and the neutral oscillatory period fluctuate, with the oscillatory period fluctuating around its value in the nonautonomous two-proneural model [Fig. 2(d)]. A similar modulation in period was recently observed in a delayed coupling model of vertebrate segmentation [26]. Numerical simulations performed for the parameter values represented by the cross signs in Fig. 7(a) confirm that the Hopf bifurcation occurs on the minus branch of Eq. (21), and that the critical intercellular signaling delay is modulated by the local-loop delay (data not shown).

Figure 8 shows the results of numerical simulations of the model equations (19) and (20) for a range of delays (τ_g and τ_f) and initial values [$A_1(0)$ and $A_2(0)$]. The behavior of this model variant is found to be qualitatively the same as that of the nonautonomous two-proneural model [Fig. 2(d)]: the Hopf bifurcation point exists on the minus branch of the eigenvalue equation [Eq. (21)] and, since the plus branch again has a positive real eigenvalue, differentiation occurs when $A_1(0) \neq A_2(0)$. However, the modulatory effect of the cell-autonomous proneural autoactivation loop, shown in Fig. 7, is seen in the comparison between the top and the middle right panels. As the local-loop delay (τ_f) increases from 0 to 15, the amplitude of oscillations decreases, as influenced by the increase in the critical signaling delay [Fig. 7(a), solid curve]. It can be seen from Fig. 7 that the cell-autonomous proneural autoactivation loops give rise to "tunability" of the oscillations.

D. Autorepression two-Hes-Her model

The autorepression two-Hes-Her model [Fig. 2(c)] is represented by the following differential equations:

$$T\dot{H}_1 = -H_1 + g(H_2(t-\tau_g))h(H_1(t-\tau_h)), \tag{23}$$

$$T\dot{H}_2 = -H_2 + g(H_1(t-\tau_g))h(H_2(t-\tau_h)). \tag{24}$$

The eigenvalue equation for the uniform steady-state solution ($H_1^* = H_2^* = H^*$) has the same form as that for the autoactivation two-proneural model [Eq. (21)],

$$1 + T\lambda = -g(H^*)\gamma^h e^{-\lambda\tau_h} \pm h(H^*)\gamma^g e^{-\lambda\tau_g}, \tag{25}$$

where, however, the definition of B is modified to be $B = -g(H^*)\gamma^h$ because h represents a decreasing Hill function.

Figure 9 shows the neutral intercellular signaling delay and the oscillatory period associated with the pure imaginary eigenvalues as a function of the delay in the local loop. The eigenvalue equation [Eq. (25)] is solved for its minus and plus branches, for the first and the second largest periods. Unlike any eigenvalue equation of the three simpler models analyzed so far [Figs. 2(b), 2(d), and 2(e)], Eq. (25) is found not to have a neutral solution when $\tau_h < 5.0483$ min.

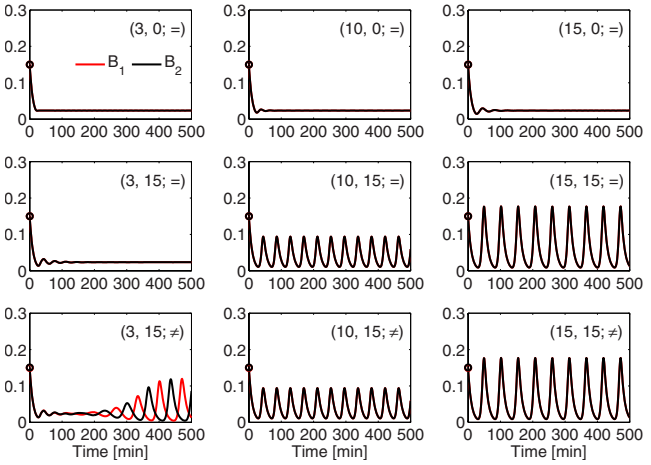

FIG. 10. (Color online) Numerical simulations of the autorepression two-Hes-Her model [Fig. 2(c)]. In comparison to Fig. 5, the behavior is found to be qualitatively different to that of the nonautonomous two-proneural model [Fig. 2(d)]. Specifically, oscillations are sustained even with nonidentical initial values, and oscillations can be out of phase as well as in phase. Values of the delays, and whether or not the initial values of H_1 and H_2 are equal, are specified in each panel as (τ_g, τ_h; =or≠).

Figure 10 shows the results of numerical simulations of the model equations (23) and (24) for a range of values of the delays (τ_g and τ_h) and initial values [$H_1(0)$ and $H_2(0)$]. These reveal two prominent features of the dynamics of this system that are qualitatively different to those of the two-proneural models [Figs. 2(b) and 2(d)]. First, oscillations can be sustained (rather than transient) even when $H_1(0) \neq H_2(0)$; second, the oscillations of H_1 and H_2 can be out of phase for certain values of the delays, as shown in the left bottom panel. Figure 11 details the transition from out-of-phase oscillations to in-phase oscillations as the value of the critical intercellular signaling delay (τ_g) increases. Strikingly, the

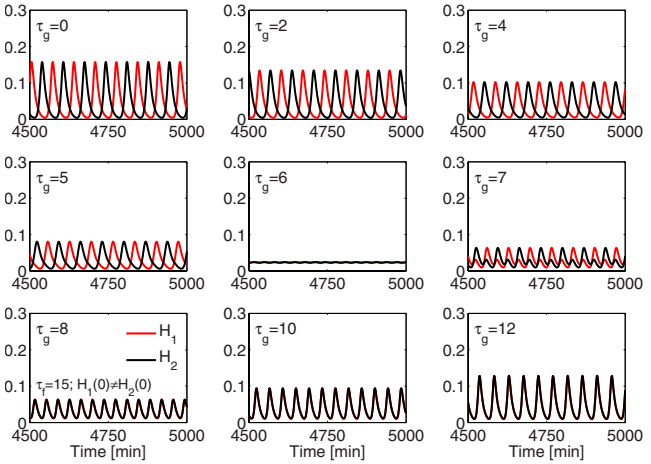

FIG. 11. (Color online) Details of the transition from out-of-phase to in-phase oscillations as the value of τ_g increases in the autorepression two-Hes-Her model [Figs. 2(c) and 10]. The transition is associated with amplitude death around $\tau_g = 6$.

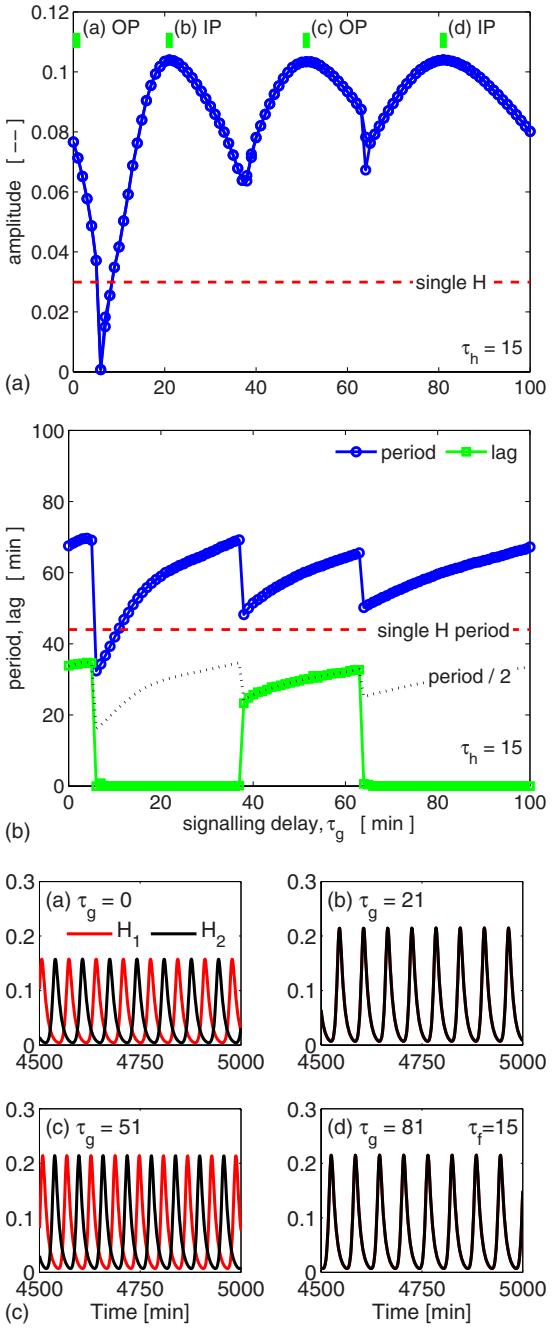

FIG. 12. (Color online) Dependence of the amplitude (top panel) and period (middle panel) of oscillatory solutions on the intercellular signaling delay (τ_g) in the autorepression two-Hes-Her model. The amplitude of an oscillatory solution is defined as the half difference between peak and trough values. The observed modulations of amplitude and period reflect the transition between out-of-phase (OP) and in-phase (IP) oscillation modes; the comparison between the lag (time difference between oscillation peaks in neighboring cells) and the half-periods of oscillations shown in the middle panel illustrates the sequential switching between out-of-phase and in-phase oscillation modes. The bottom four panels show time courses obtained by numerical simulation of Eqs. (23) and (24) at the four values of τ_g marked in the top panel. The first transition corresponds to Fig. 11. The dashed lines in the top and the middle panels represent, respectively, the amplitude and the period in the single-cell Hes-Her model with a local delay $\tau_h=15$.

transition is found to be associated with a pointwise amplitude death [27]. The transition found in numerical simulations with various τ_h is compared to the neutral properties estimated by the linear analysis in Fig. 9. In a cell-autonomous Hes-Her oscillator, the oscillatory period increases monotonically with delay [18], while for the coupled cells to cycle out of phase, the signaling delay must be about half a period. Therefore the monotonic increase in the critical τ_g and in the critical period (T_c) suggests that the overall network behavior of the autorepression two-Hes-Her model is controlled by the two local autonomous Hes-Her oscillators.

In contrast, when the intercellular signaling delay (τ_g) is varied while the local delay (τ_h) is kept constant, transitions between in-phase and out-of-phase modes occur sequentially and are associated with modulations in amplitude and period (Fig. 12). The mode transitions repeat as τ_g is increased, but not in an identical manner. Unlike the first transition shown in Fig. 11, a clear amplitude death is not observed at higher-order transitions. Further examination reveals that the sequential transitions are not induced by the network structure of two mutually repressive autonomous oscillators, but by the structure of two mutually influencing autonomous oscillators, forming an overall positive feedback loop. Indeed, when intercellular interactions are modeled by an increasing Hill function that represents activation, the transition still occurs, but in a reverse order, starting from the in-phase mode at $\tau_g=0$ (data not shown).

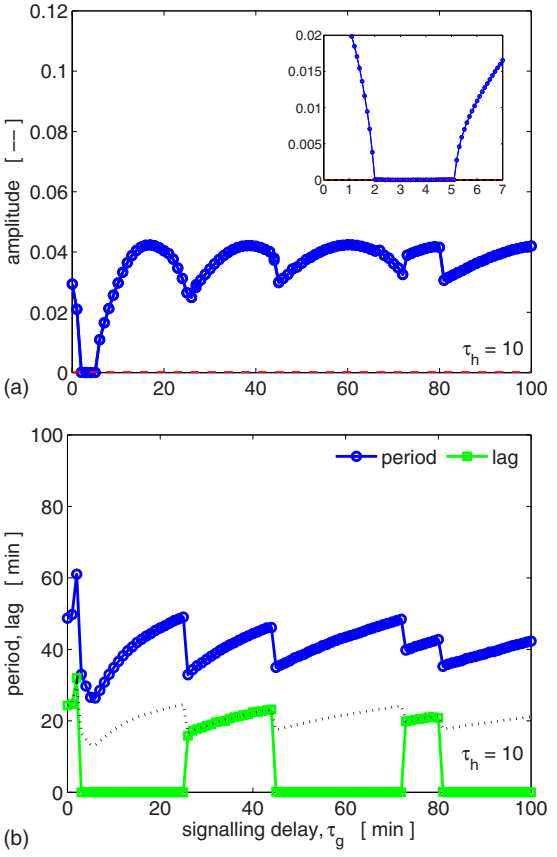

FIG. 13. (Color online) Coupled subcritical oscillators illustrating a finite-τ_g-range oscillation death. The inset in the top panel shows the oscillation death in detail.

The intercellular coupling is found to have additional dynamical consequences. While an isolated cell containing the Hes-Her feedback loop cannot exhibit sustained oscillations when the delay (τ_h) is below its critical value, such a local-loop critical delay ($\tau_{h\ \mathrm{cr}}$) can be lowered by the intercellular coupling, as shown in Fig. 13, where $\tau_h = 10 < \tau_{h\ \mathrm{cr}} = 13.0548$. Furthermore, oscillation death is found to happen in a definite range of the intercellular signaling delay (τ_g).

The three features observed in numerical simulations—the oscillation in an originally subcritical delay range ($\tau_h < \tau_{h\ \mathrm{cr}}$), the transition between out-of-phase and in-phase oscillatory modes, and the finite-τ_g-range oscillation death—can be understood analytically as follows. Linearization of Eqs. (23) and (24) around the uniform steady state yields

$$\begin{pmatrix} 1 + T\lambda + \alpha & \beta \\ \beta & 1 + T\lambda + \alpha \end{pmatrix} \begin{pmatrix} \bar{H}_1 \\ \bar{H}_2 \end{pmatrix} = \mathbb{M} \begin{pmatrix} \bar{H}_1 \\ \bar{H}_2 \end{pmatrix} = \begin{pmatrix} 0 \\ 0 \end{pmatrix}, \tag{26}$$

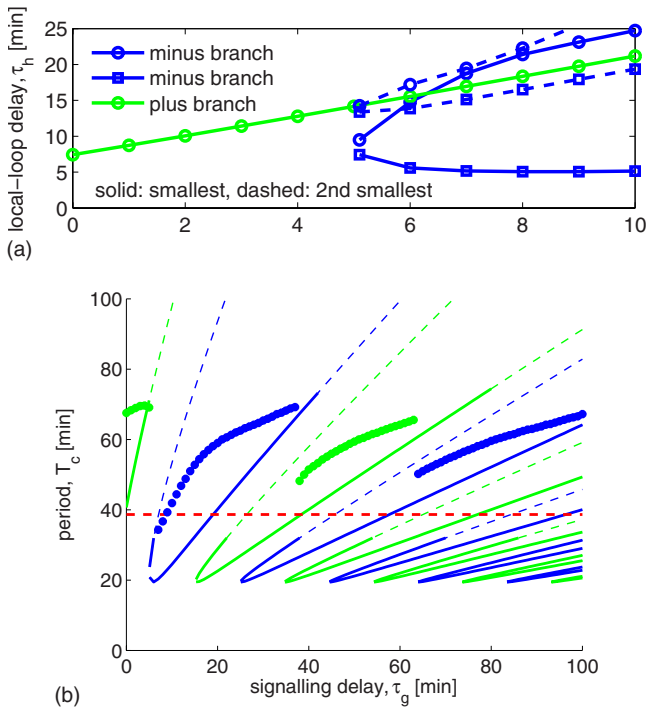

FIG. 14. (Color online) The origin of oscillation death and the transition between the out-of-phase and the in-phase oscillatory modes in the autorepression two-Hes-Her model [Fig. 2(c)]. Neutral local-loop delay (upper panel) and oscillatory period (lower panel) are shown as functions of the intercellular signaling delay τ_g. The eigenvalue equation [Eq. (25)] is solved numerically for its minus and plus branches. Neither the out-of-phase nor the in-phase branch has a solution for $\tau_h = 10$ for $2 \leq \tau_g < 5.1$, corresponding to the oscillation death observed in Fig. 13. Simulated periods for $\tau_h = 15$ (shown also in Fig. 12, middle panel) are shown by blue and green dots in the lower panel, where the neutral period obtained by linear stability analysis is shown by solid and dashed curves (corresponding to the neutral delay being smaller or larger than $\tau_h = 15$, respectively). Note the different horizontal scales in the two panels.

where $\alpha = g(H^*)\gamma^h e^{-\lambda\tau_h}$ and $\beta = h(H^*)\gamma^g e^{-\lambda\tau_g}$. The associated eigenvalue equation, given by $\det \mathbb{M} = 0$, is

$$1 + T\lambda = -\alpha \pm \beta, \tag{27}$$

which is the same as Eq. (25). By substituting Eq. (27) into Eq. (26), it can be seen that the plus branch is associated with the out-of-phase oscillation mode: $(\bar{H}_1, \bar{H}_2) = (1, -1)$, whereas the minus branch is associated with the in-phase oscillation mode: $(\bar{H}_1, \bar{H}_2) = (1, 1)$. Numerical evaluation of the eigenvalue equation yields the relations between the neutral delay in the local loop ($\tau_{h\ \mathrm{cr}}$) and the intercellular signaling delay (τ_g) shown in Fig. 14, for both the out-of-phase and the in-phase modes. For example, for $\tau_h = 10$ (Fig. 13), when $0 < \tau_g < 2$ only the out-of-phase mode is allowed, whereas when $\tau_g \geq 5.1$ only the in-phase mode is allowed. In between ($2 < \tau_g < 5.1$), no oscillation is allowed, explaining the origin of the oscillation death shown in Fig. 13. However, the comparison of periods to simulation results in the lower panel shows that as τ_g increases, more and more branches appear, and the model behavior becomes more nonlinear. The actual transitions observed in simulations do not coincide with the boundaries between the regions that linear stability analysis predicts to be competent (solid curve) and incompetent (dashed curve) for sustained oscillations.

It is striking that, only by changing the local loop attached to the nonautonomous two-X model from autoactivation [Fig. 2(b), where X is proneural] to autorepression [Fig. 2(c), where X is Hes-Her], the network behavior changes completely. This simple example, motivated by the structure of the neural differentiation network, highlights the importance

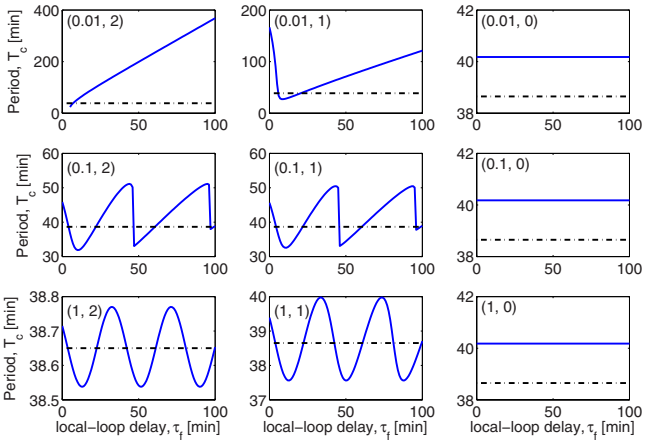

FIG. 15. (Color online) The largest neutral period (T_c) associated with the eigenvalues of the autorepression two-Hes-Her model [Fig. 2(c)] for different values of the threshold (K_h) and the Hill coefficient (ν_h) in the local feedback loop. As K_h increases, the behavior of this model becomes similar to that of the autoactivation two-proneural model [Fig. 2(b)], while as ν_h decreases, the behavior becomes similar to that of the nonautonomous two-proneural model [Fig. 2(d)]. Note the different vertical scales in each plot. The dashed-dotted line in each panel represents the critical period in the nonautonomous two-cell model. Varied parameters are given in each panel as (K_h, ν_h).

of examining in detail the structure of any gene regulatory network, even if it is centered on a small and seemingly simple motif.

The richness in the behavior of this autorepression two-Hes-Her model can be seen in Fig. 15, where the largest neutral period (T_c) associated with the eigenvalues is plotted for different values of the threshold (K_h) and Hill coefficient (ν_h) in the local feedback loop. As K_h increases, the behavior of this model becomes similar to that of the autoactivation two-proneural model [Fig. 2(b)], while as ν_h decreases, the behavior becomes similar to that of the nonautonomous two-proneural model [Fig. 2(d)].

V. EXTENSION TO *N*-CELL RING MODEL

The two-cell models discussed so far can be naturally extended to one-dimensional arrays of cells. To avoid potential boundary effects, we consider the specific case of a ring of N cells labeled with a single index $i=1,2,\ldots,N$ (i.e., a line of cells with periodic boundary conditions imposed). As an example, we study the autorepression Hes-Her model. We assume that each cell signals equally to both its nearest neighbors, yielding the following model equations:

$$T\dot{H}_i = -H_i + h(H_i(t-\tau_h))g\left(\frac{H_{i-1}(t-\tau_g)+H_{i+1}(t-\tau_g)}{2}\right), \tag{28}$$

where i denotes cell number and the imposition of periodic boundary conditions implies that $H_{-1}=H_N$ and $H_{N+1}=H_1$. Linearizing Eq. (28) around the uniform steady-state solution ($H_i=H^*$) by expanding H_i as $H_i=H^*+\bar{H}_i e^{\lambda t}$ yields the following eigenvalue equations:

$$0 = A\bar{H}_{i-1} + (B-\lambda T)\bar{H}_i + A\bar{H}_{i+1}, \quad i=1,2,\ldots,N, \tag{29}$$

where

$$A(\lambda) = -\tfrac{1}{2}h(H^*)\gamma^g e^{-\lambda\tau_g},$$

$$B(\lambda) = -1 - g(H^*)\gamma^h e^{-\lambda\tau_h}.$$

Equation (29) can be represented in matrix form as

$$\begin{pmatrix} 0 \\ 0 \\ 0 \\ \vdots \\ 0 \end{pmatrix} = \begin{pmatrix} B-\lambda T & A & 0 & 0 & 0 & \cdots & 0 & 0 & A \\ A & B-\lambda T & A & 0 & 0 & \cdots & 0 & 0 & 0 \\ 0 & A & B-\lambda T & A & 0 & \cdots & 0 & 0 & 0 \\ & & & & & \cdots & & & \\ A & 0 & 0 & 0 & 0 & \cdots & 0 & A & B-\lambda T \end{pmatrix} \begin{pmatrix} \bar{H}_1 \\ \bar{H}_2 \\ \bar{H}_3 \\ \vdots \\ \bar{H}_N \end{pmatrix} = \mathbb{M} \begin{pmatrix} \bar{H}_1 \\ \bar{H}_2 \\ \bar{H}_3 \\ \vdots \\ \bar{H}_N \end{pmatrix}, \tag{30}$$

where it is important to note that A and B are nonpolynomial functions of λ. The eigenvalues λ are determined by $\det \mathbb{M}=0$.

We first note that the phase relations between adjacent cells in oscillatory solutions can be determined from the form of the eigenvector $(\bar{H}_1,\bar{H}_2,\ldots,\bar{H}_N)$ corresponding to each eigenvalue. For any value of N, Eq. (30) has an eigenvector $(1,1,\ldots,1)$ with an eigenvalue determined by the solutions of $T\lambda=B+2A$. This corresponds to an oscillatory mode where all cells are in phase. Furthermore, for any even value of N, Eq. (30) has an eigenvector $(1,-1,1,\ldots,1,-1)$ with an eigenvalue determined by the solutions of $T\lambda=B-2A$. This corresponds to an oscillatory mode where all cells are out of phase. These two cases are simple extensions of the dynamics observed in the two-cell model.

To illustrate potential extensions to the dynamics observed in the two-cell model, we consider the specific case $N=4$,

$$\mathbb{M} = \begin{pmatrix} B-\lambda T & A & 0 & A \\ A & B-\lambda T & A & 0 \\ 0 & A & B-\lambda T & A \\ A & 0 & A & B-\lambda T \end{pmatrix}, \tag{31}$$

and

$$\det \mathbb{M} = (-2A+T\lambda-B)(2A+T\lambda-B)(-B+T\lambda)^2.$$

Therefore, the eigenvalues are determined by the solutions of

$$T\lambda = B \mp 2A, \tag{32}$$

$$T\lambda = B. \tag{33}$$

The explicit expression of Eqs. (32) and (33) are found to be the same as the eigenvalue equations derived for the autorepression two-Hes-Her model [Eq. (25)], and for the autorepression single-Hes-Her model [the minus branch of Eq. (13)], respectively.

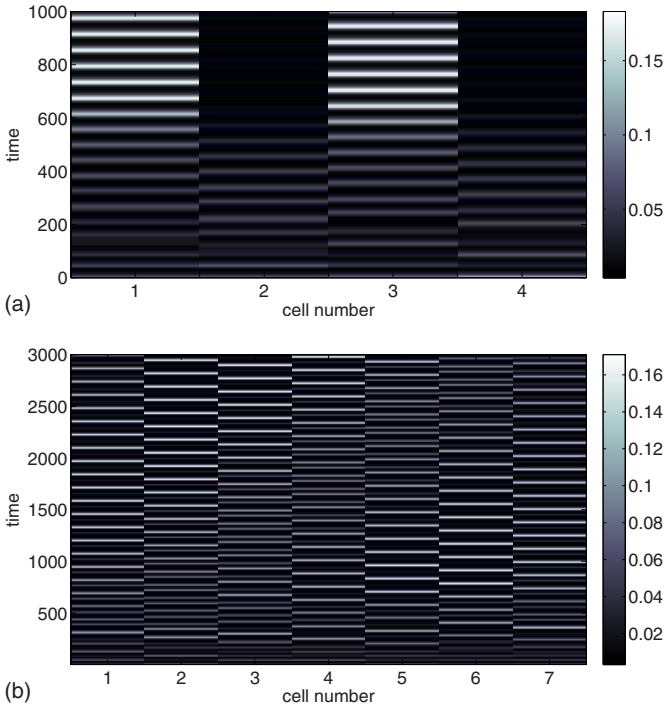

FIG. 16. (Color online) Complex oscillatory dynamics in one-dimensional arrays of coupled cells. Simulations of Eqs. (28), representing the autorepression Hes-Her model in a ring of N cells. Simulations were carried out using the standard parameter values (Table I) with $\tau_h=20$, $\tau_g=8$, and with initial history $H_i(t)=0.1+0.1\xi_i$ for $-\max(\tau_g,\tau_h)\leq t\leq 0$, where ξ_i are drawn from independent uniform distributions on [0,1]. (a) Amplitude death combined with out-of-phase oscillations: $N=4$. (b) Complex dynamics resulting from mode interactions: $N=7$.

As above, the phase relations between adjacent cells in oscillatory solutions can be determined from the form of the eigenvector $(\bar{H}_1,\bar{H}_2,\bar{H}_3,\bar{H}_4)$ corresponding to each eigenvalue. From Eq. (31), the eigenvector on the minus branch of Eq. (32) is found to be $(1,-1,1,-1)$, representing the out-of-phase oscillatory mode, while the eigenvector on the plus branch is (1,1,1,1), representing the in-phase mode. In contrast, the eigenvector associated with Eq. (33), which is present when $N=4,8,16,\ldots$, is found to be $(1,0,-1,0)$, representing amplitude death for every other cell in the array, with the remaining cells being out of phase. This is a unique dynamical feature that the two-cell model fails to capture. An example of this mode for $N=4$ is shown in Fig. 16(a).

For larger values of N, the interaction between multiple modes can result in a more complex oscillatory behavior, in which waves of phase and amplitude differences can propagate around the ring. Furthermore, the oscillatory profile for each cell is often complex, with multiple peaks per oscillatory period and "intermittent" oscillations being common. An example for $N=7$ is shown in Fig. 16(b). These features are also observed in simulations on regular square and hexagonal two-dimensional arrays of cells (results not shown).

VI. ANALYSIS AND REDUCTIONS IN THE FULL Hes-Her–PRONEURAL MODEL

In this section, from the viewpoint of eigenvalue equations, it is discussed how the full Hes-Her–proneural model [Fig. 2(a)] is related to the autoactivation proneural model [Fig. 2(b)] and to the autorepression Hes-Her model [Fig. 2(c)]. For the uniform steady-state solution $(H_1^*=H_2^*=H^*,\ A_1^*=A_2^*=A^*)$ of the full Hes-Her–proneural model, the eigenvalue equation is derived from its model equations (1)–(4) to be

$$(1+T_H\lambda+ae^{-\lambda\tau_3})(1+T_A\lambda-ce^{-\lambda\tau_4})=\pm bde^{-\lambda\tau_{tot}}, \tag{34}$$

where $a=f_1(A^*)\gamma^{g_2}$, $b=f_2(A^*)\gamma^{g_1}$, $c=g_1(H^*)\gamma^{f_2}$, $d=g_2(H^*)\gamma^{f_1}$, and $\tau_{tot}=\tau_1+\tau_2$.

First, explicit forms of the neutral angular frequency (ω_c) and delay (τ_{tot}) are derived for a simple example, where $T_A=T_H=T$, $\tau_3=\tau_4=\tau_a$, and $f_1=f_2=g_1=g_2$. The last assumption means that K and ν are, respectively, the same all in f_1, f_2, g_1, and g_2. Then, from Eqs. (9) and (10), $A^*=H^*$, and consequently $a=c=b=d:=\phi$. Therefore, Eq. (34) becomes

$$1+2T\lambda+T^2\lambda^2-\phi^2e^{-2\lambda\tau_a}=\pm\phi^2e^{-\lambda\tau_{tot}}. \tag{35}$$

For a neutral solution, Eq. (35) becomes

$$(1-T^2\omega^2-\phi^2\cos 2\omega\tau_a)^2+(2T\omega+\phi^2\sin 2\omega\tau_a)^2=\phi^4, \tag{36}$$

$$\tan\omega\tau_{tot}=\mp\frac{2T\omega+\phi^2\sin 2\omega\tau_a}{1-T^2\omega^2-\phi^2\cos 2\omega\tau_a}:=\mp\Delta. \tag{37}$$

For the plus branch in Eq. (34),

$$\tau_{tot}=\frac{1}{\omega}\max[\tan^{-1}(-\Delta),\pi+\tan^{-1}(-\Delta)], \tag{38}$$

whereas for the minus branch in Eq. (34),

$$\tau_{tot}=\frac{1}{\omega}\max[\tan^{-1}(+\Delta),\pi+\tan^{-1}(+\Delta)]. \tag{39}$$

Figure 17 shows the neutral (a) intercellular signaling delay and (b) period, as a function of the local-loop delay (τ_a). The eigenvalue equation [Eq. (35)] is solved for its minus and plus branches, for the first and the second largest periods. In comparison to Figs. 7 and 9, the autorepression two-Hes-Her circuit component is found to be dominant in this full Hes-Her–proneural model, although the neutral values are found to exist for any τ_a, unlike in the autorepression two-Hes-Her model, where no pure imaginary solution can exist for τ_f less than 5.0483 (τ_f corresponds to τ_a in this section).

In the following, based on the eigenvalue equation of the full Hes-Her–proneural model [Eq. (34)], we clarify the conditions under which this full Hes-Her–proneural model can be reduced to the autoactivation two-proneural model [Fig. 2(b)] and to the autorepression two-Hes-Her model [Fig. 2(c)].

A. Reduction to the autoactivation two-proneural model

The eigenvalue equation of the full Hes-Her–proneural model [Eq. (34)] is reduced to the eigenvalue equation of the autoactivation two-proneural model [Eq. (21)] when (a) T_H

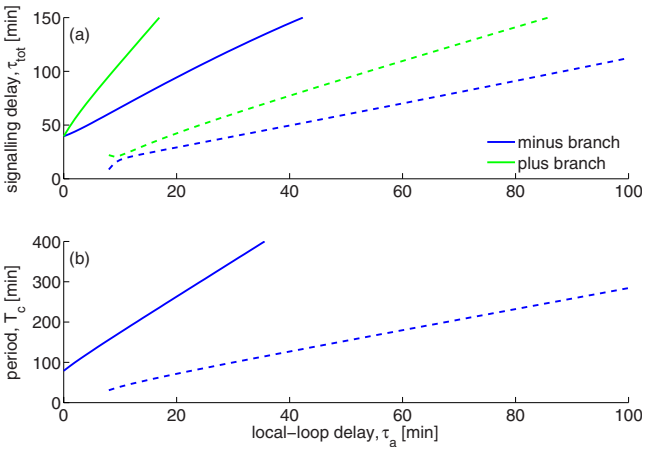

FIG. 17. (Color online) Neutral (a) intercellular signaling delay and (b) period, associated with the pure imaginary eigenvalues of the full Hes-Her–proneural model, shown as a function of the local-loop delay. The eigenvalue equation [Eq. (35)] is solved for its minus and plus branches, for the first and the second largest periods (solid and dashed lines, respectively). In comparison to Figs. 7 and 9, the autorepression two-Hes-Her circuit component is found to be dominant in this full Hes-Her–proneural model.

$=0$, (b) $\gamma^{g_2}=0$, (c) $H^*=A^*$, (d) $g_2(H^*)\gamma^{f_1}=1$, and (e) $\tau_1=0$. These conditions must hold irrespective of whether f_i and g_i are Hill functions or not. If Hill functions $f(x,K,\nu)$ and $g(x,K,\nu)$, where K and ν are the scaled threshold and the Hill coefficient, are employed, condition (b) can be met by setting K in g_2 to be $+\infty$. Because this operation makes $g_2(H^*)=1$, from the steady-state solution of the full model $[H^*=f_1(A^*)g_2(H^*)]$, condition (c) is found to require that f_1 is not a Hill function but a linear function: $f_1(x)=x$, whereby $\gamma^{f_1}=1$, making all five conditions satisfied. The last operation $[f_1(x)=x]$ means that for a sequence of two functions f and g to be represented only by g, f needs to be $f(x)=x$. In short, the autoactivation two-proneural model [Eqs. (19) and (20)] is obtained by assuming the following conditions on the full Hes-Her–proneural model [Eqs. (1)–(4)]: the activation from a proneural protein $(A_{i=1,2})$ to the adjacent Hes-Her $(H_{i=2,1})$ is linear and instantaneous and Hes-Her is not associated with an autorepression loop.

B. Reduction to the autorepression two-Hes-Her model

The eigenvalue equation of the full Hes-Her–proneural model [Eq. (34)] is reduced to the eigenvalue equation of the autorepression two-Hes-Her model [Eq. (25)] when (a) $T_A=0$, (b) $\gamma^{f_2}=0$, (c) $f_1(A^*)=g_1(H^*)$, (d) $f_2(A^*)\gamma^{f_1}=1$, and (e) $\tau_1=0$. These conditions must hold irrespective of whether f_i and g_i are Hill functions or not. If Hill functions are employed, condition (b) can be met by setting K in f_2 to be 0. Because this operation makes $f_2(A^*)=1$, from the steady-state solution of the full model $[A^*=g_1(H^*)f_2(A^*)]$, condition (c) is found to require that f_1 is not a Hill function but a linear function: $f_1(x)=x$, whereby $\gamma^{f_1}=1$, making all five conditions.

VII. GENERAL DISCUSSION

The development of multicellular organisms is a process of sequential and concurrent cell differentiations, the timings of which must be tightly controlled. Recent experimental studies have revealed that in the case of vertebrate neural differentiation, cell differentiation can occur after a transient oscillation in cell state [22]. Since neural differentiation in vertebrates occurs over a considerable time interval, these transient oscillations may play a role in the scheduling of neural differentiation in relation to other developmental events. The occurrence of such transient oscillations on the route to neural differentiation was previously predicted in a simple delay model of Delta-Notch-mediated lateral inhibition [15].

In the present study, we have analyzed a more detailed model of the neural differentiation network. The model has a nested-loop structure, with intercellular signaling (as mediated by interactions between DSL ligands and Notch family receptors) coupled to local cell-autonomous feedback loops. Using a combination of stability analysis and numerical simulation, we have shown that the incorporation of local feedback loops has potentially significant impacts on the dynamics of the signaling network. In particular, the time delays in the local feedback loops were found to play a central role in controlling the behavior of the whole network whether it heads toward differentiation, whether it shows an oscillation, or whether such an oscillation is sustained or transient, as well as providing tunability in the amplitude and period of oscillations.

Many classes of autoregulatory genes have been identified. Because these genes are also nodes in larger genetic regulatory networks, nested feedback loop structures are rather common. The results of the present study highlight the need for careful examination of the predictions made by nondelay network models, which include the *Drosophila* neurogenic model studied by Meir *et al.* that yielded a conclusion that the total system was robust to local changes to the network circuitry [10].

In a more general perspective, a biological system is known to involve a relatively small number of genes, having numerous features and functions. Some of the present functions may have been acquired by the addition of a few local loops to the old conserved ones. Moreover, because the loops considered in the present study are all very simple, the outcomes of the present study may have relevance to nonbiological systems as well.

[1] J. J. Tyson, K. C. Chen, and B. Novak, Curr. Opin. Cell Biol. **15**, 221 (2003).
[2] K. Kruse and F. Jülicher, Curr. Opin. Cell Biol. **17**, 20 (2005).
[3] J. L. Cherry and F. R. Adler, J. Theor. Biol. **203**, 117 (2000).
[4] J. E. Ferrell, Jr., Curr. Opin. Cell Biol. **14**, 140 (2002).
[5] S. Artavanis-Tsakonas, M. D. Rand, and R. J. Lake, Science **284**, 770 (1999).
[6] J. Lewis, Semin. Cell Dev. Biol. **9**, 583 (1998).
[7] A. Louvi and S. Artavanis-Tsakonas, Nat. Rev. Neurosci. **7**, 93 (2006).
[8] G. S. Richards, E. Simionato, M. Perron, M. Adamska, M. Vervoort, and B. M. Degnan, Curr. Biol. **18**, 1156 (2008).
[9] J. R. Collier, N. A. M. Monk, P. K. Maini, and J. H. Lewis, J. Theor. Biol. **183**, 429 (1996).
[10] E. Meir, G. von Dassow, E. Munro, and G. M. Odell, Curr. Biol. **12**, 778 (2002).
[11] N. Bertrand, D. S. Castro, and F. Guillemot, Nat. Rev. Neurosci. **3**, 517 (2002).
[12] R. Kageyama, T. Ohtsuka, and T. Kobayashi, Development **134**, 1243 (2007).
[13] J. M. Mahaffy and C. V. Pao, J. Math. Biol. **20**, 39 (1984).
[14] J. M. Mahaffy, Math. Biosci. **90**, 519 (1988).
[15] S. R. Veflingstad, E. Plahte, and N. A. M. Monk, Physica D **207**, 254 (2005).
[16] M. H. Jensen, K. Sneppen, and G. Tiana, FEBS Lett. **541**, 176 (2003).
[17] J. Lewis, Curr. Biol. **13**, 1398 (2003).
[18] N. A. M. Monk, Curr. Biol. **13**, 1409 (2003).
[19] H. Momiji and N. A. M. Monk, J. Theor. Biol. **254**, 784 (2008).
[20] H. Hirata, S. Yoshiura, T. Ohtsuka, Y. Bessho, T. Harada, K. Yoshikawa, and R. Kageyama, Science **298**, 840 (2002).
[21] Y. Masamizu, T. Ohtsuka, Y. Takashima, H. Nagahara, Y. Takenaka, K. Yoshikawa, H. Okamura, and R. Kageyama, Proc. Natl. Acad. Sci. U.S.A. **103**, 1313 (2006).
[22] H. Shimojo, T. Ohtsuka, and R. Kageyama, Neuron **58**, 52 (2008).
[23] J. T. Nichols, A. Miyamoto, and G. Weinmaster, Traffic (Oxford, U. K.) **8**, 959 (2007).
[24] U. Alon, Nat. Rev. Genet. **8**, 450 (2007).
[25] J. M. D. Vosper, C. S. Fiore-Heriche, I. Horan, K. Wilson, H. Wise, and A. Philpott, Biochem. J. **407**, 277 (2007).
[26] L. G. Morelli, S. Ares, L. Herrgen, C. Schröter, F. Jülicher, and A. C. Oates, HFSP J. **3**, 55 (2009).
[27] D. V. Ramana Reddy, A. Sen, and G. L. Johnston, Phys. Rev. Lett. **80**, 5109 (1998).